A peer-reviewed version of this preprint was published in PeerJ on 13 March 2014.

<u>View the peer-reviewed version</u> (peerj.com/articles/305), which is the preferred citable publication unless you specifically need to cite this preprint.

Joshi A, Esteve V, Buckroyd AN, Blatter M, Allain FH-, Curry S. 2014. Solution and crystal structures of a C-terminal fragment of the neuronal isoform of the polypyrimidine tract binding protein (nPTB) PeerJ 2:e305 https://doi.org/10.7717/peerj.305

- 1 Solution and crystal structures of a C-terminal fragment of the neuronal
- 2 isoform of the polypyrimidine tract binding protein (nPTB)

- 4 Amar Joshi^{1*‡}, Vicent Esteve^{2#‡}, Adrian N. Buckroyd^{1‡}, Markus Blatter², Frédéric H.-
- 5 T. Allain^{2†}, Stephen Curry^{1†}

6

- 7 Department of Life Sciences, Imperial College, Exhibition Road, London SW7 2AZ,
- 8 United Kingdom. ²Institute of Molecular Biology and Biophysics, ETH Zürich,
- 9 Switzerland.
- 10 *Present address: Department of Biochemistry, Henry Wellcome Building, University
- of Leicester, Lancaster Road, Leicester LE1 9HN, United Kingdom. *Present address:
- 12 CIBER-BBN, Dep. Quimica Fisica, Universitat de Valencia, Dr. Moliner, 50 46100-
- Burjassot, Valencia, Spain. *Present address: Department of Biochemistry, University
- of Cambridge, Tennis Court Road, CB2 1QW, United Kingdom.
- [‡]These authors contributed equally to this work.

16

17 [†]Corresponding authors:

- 18 Frédéric H.-T. Allain, Institute of Molecular Biology and Biophysics, ETH Zürich,
- 19 Switzerland. Tel: +41 44 633 3940; email: allain@mol.biol.ethz.ch
- 20 Stephen Curry, Department of Life Sciences, Imperial College, Exhibition Road,
- 21 London SW7 2AZ, United Kingdom. Tel: +44 20 7594 7632; email:
- 22 s.curry@imperial.ac.uk

Joshi et al.

Abstract

The eukaryotic polypyrimidine tract binding protein	(PTB) serves primarily as a
regulator of alternative splicing of messenger RNA,	but is also co-opted to other roles
such as RNA localisation and translation initiation fr	om internal ribosome entry sites.
The neuronal paralogue of PTB (nPTB) protein is 75	5% identical in amino acid
sequence with PTB. Although the two proteins have	broadly similar RNA binding
specificities and effects on RNA splicing, differentia	al expression of PTB and nPTB
can lead to the generation of alternatively spliced m	RNAs. RNA binding by PTB and
nPTB is mediated by four RNA recognition motifs (RRMs). We present here the
crystal and solution structures of the C-terminal dom	nain of nPTB (nPTB34) which
contains RRMs 3 and 4. As expected the structures a	are similar to each other and to the
solution structure of the equivalent fragment from P	ΓB (PTB34). The result confirms
that, as found for PTB, RRMs 3 and 4 of nPTB inter	act with one another to form a
stable unit that presents the RNA-binding surfaces of	f the component RRMs on
opposing sides. The major differences between PTB	34 and nPTB34 arise from amino
acid side chain substitutions on the exposed β -sheet	surfaces and adjoining loops of
each RRM, which are likely to modulate interactions	s with RNA.

Introduction

43	Alternative splicing is the rule rather than the exception in the human genome. Over
44	95% of multi-exon genes produce alternatively spliced mRNAs (Nilsen & Graveley,
45	2010), yielding many more protein variants or isoforms than specified by the number
46	of genes. The process of alternative splicing is controlled by regulatory sequences
47	within pre-mRNA transcripts that recruit suites of proteins to determine whether
48	selected exons are included or excluded as mRNA is brought to maturity.
49	The polypyrimidine tract binding protein (PTB) is a well-characterized regulator of
50	alternative splicing (Garcı́a-Blanco, Jamison & Sharp, 1989; Gil et al., 1991) although
51	it also has significant roles that affect the processing, localization and use of a variety
52	of mRNAs [reviewed by (Sawicka et al., 2008)]. PTB does not recognize a unique
53	RNA sequence; rather it is specific for short motifs (e.g. UCUCU, UCUU) within
54	pyrimidine rich regions of pre-mRNA (Singh, Valcárcel & Green, 1995; Pérez et al.,
55	1997). In alternative splicing, PTB binding is most commonly associated with
56	exclusion or skipping of the regulated exon, although more recent genome-wide
57	splicing studies have indicated that PTB binding can also promote exon inclusion in a
58	minority of cases (Xue et al., 2009; Llorian et al., 2010; Witten & Ule, 2011).
59	Three tissue-specific homologues of PTB have been identified $-\ \mathrm{smPTB}$, ROD1 and
60	nPTB — all of which have high levels of amino acid sequence identity with the
61	prototypical protein (69-74%) and are therefore likely to have very similar structures.
62	\mbox{smPTB} (smooth muscle tissue) has so far only been found in rodents (Gooding, Kemp
63	& Smith, 2003), whereas the homologue ROD1 is expressed primarily in
64	hematopoietic tissues (Yamamoto et al., 1999). nPTB is found predominantly in brain
65	and testis but also, at low levels, in muscle cells (Markovtsov et al., 2000; Polydorides
66	et al., 2000).
67	PTB and nPTB bind to the same RNA sequences and have similar effects on
68	alternative splicing events for a number of transcripts (Markovtsov et al., 2000;
69	Pilipenko et al., 2001; Spellman, Llorian & Smith, 2007). However, for some
70	neuronal-specific alternative splicing events the expression of nPTB leads to distinct
71	outcomes. For example, the tyrosine kinase c - src has an n - src isoform found only in
72	brain tissue that requires nPTB for the selective inclusion of a neuronal-specific exon
73	(Markovtsov et al., 2000; Sharma, Falick & Black, 2005; Boutz et al., 2007).

74	PTB (and its homologues) contain 4 RNA recognition motif domains (RRMs)
75	separated by long flexible linkers and arrayed, when not bound to RNA, in a relatively
76	extended, linear conformation (Petoukhov et al., 2006). The solution structures of
77	each RRM have been solved in the absence (Conte et al., 2000; Simpson et al., 2004;
78	Vitali et al., 2006) and presence (Oberstrass et al., 2005) of RNA. While RRMs 1 and
79	4 adopt a canonical $\beta\alpha\beta\beta\alpha\beta$ topology with two helices packed against a four-strand
80	β -sheet that forms the primary RNA binding surface, RRMs 2 and 3 have a modified
81	architecture. In these domains a C-terminal extension beyond $\beta 4$ loops across the
82	upper edge of the β -sheet and adds a fifth strand on the far side of the sheet; this
83	expands the size of the RNA binding platform, while the $\beta4$ - $\beta5$ loop provides
84	additional points of interaction with RNA (Conte et al., 2000; Simpson et al., 2004;
85	Oberstrass et al., 2005).
86	The α-helical regions of RRMs 3 and 4 pack together to form a stable unit in which
87	the RNA-binding β -sheets are exposed on opposite sides; it has been proposed that
88	this configuration enforces looping of RNA that plays an important role in defining
89	exon structures to be excised from pre-mRNA (Oberstrass et al., 2005; Vitali et al.,
90	2006; Lamichhane et al., 2010). Although early studies had suggested that RRM3 and
91	RRM4 might not interact at physiological salt concentrations (Conte et al., 2000;
92	Clerte & Hall, 2006), it is now generally accepted that this pair of RRMs have fixed
93	relative orientations (Lamichhane et al., 2010; Maynard & Hall, 2010). Evidence
94	suggests that the RRM1 and RRM2 bind RNA as individual domains although RRM2
95	is also involved in protein-protein interactions with the splicing co-regulator Raver1
96	(Rideau et al., 2006). Crystallographic analysis has revealed how the helical face of
97	the PTB RRM2 provides a binding surface for specific recognition of specific peptide
98	motifs in Raver1 (Joshi et al., 2011).
99	Although PTB and nPTB are likely to have similar structures because of their high
100	sequence identity (75%) (Fig. 1a), to begin to tease out the structural basis for
101	observed differences in splicing regulation we have determined the structure of a C-
102	terminal fragment of nPTB that contains RRMs 3 and 4 (nPTB34). We have solved
103	the structures both crystallographically and by NMR. Here we compare those
104	structures with each other and with the solution structure of the equivalent fragment
105	from PTB isoform1 (called here PTB34).

Structure of nPTB34 Page 5/25 Joshi et al.

106

107

Results and Discussion

108	Crystal Structure of nPTB34
109	nPTB34, a C-terminal nPTB fragment that contains RRMs 3 and 4 (residues 336-531)
110	was over-expressed in E. coli, purified and crystallized by sitting drop vapor diffusion
111	in 20% PEG 6000, 0.1 Tris pH 8.0 with 2 mM $ZnCl_2$ as an additive (see Materials and
112	Methods). The crystals diffracted X-rays to 1.7 Å and were found to belong to space-
113	group P1. Attempts to phase the diffraction data by molecular replacement using the
114	solution structure of PTB34 (Vitali et al., 2006) were unsuccessful. Instead, phases
115	were obtained by multi-wavelength anomalous dispersion (MAD) using data collected
116	from a crystal of Se-Met-labeled nPTB34. This produced a high-quality electron
117	density map that revealed a total of eight nPTB34 molecules in the asymmetric unit
118	(Fig. 1b). The eight polypeptide chains were built almost in their entirety; due to poor
119	electron density residue 336 at the start of nPTB34 was omitted, as were residues 420-
120	423 (and one or two flanking residues in some chains) at the C-terminal end of the $\beta4$
121	$\beta 5$ loop of RRM3. The final model, which incorporates 1099 water molecules, was
122	refined to an R_{free} of 27.3% with good stereochemistry (Fig. 1c). Full data collection
123	and refinement statistics are given in Table 1.
124	The structures of the eight copies of nPTB34 within the asymmetric unit of our
125	crystals are very similar to one another (Fig. 1d). Pairwise superpositions of the eight
126	chains give an average root-mean-square deviation (RMSD) for \boldsymbol{C}_{α} atoms of only
127	0.17 Å. This is not surprising since the unit cell parameters deviate only marginally
128	from a P2 ₁ 2 ₁ 2 space group (see Materials and Methods); what this means is that there
129	are only two positions in the asymmetric unit, exemplified by chains A, B, E and F on
130	the one hand and C, D, G and H on the other, that have significantly different packing
131	environments.
132	Each molecule in the asymmetric unit is associated with a Zn ²⁺ ion that mediates
133	crystal-packing contact between His 412 from one chain and His 491 of a neighboring
134	molecule (e.g. between chains A and C within the asymmetric unit). The tetrahedral
135	coordination required by zinc appears to be completed by a Cl ⁻ ion and a water
136	molecule. Four additional crystal contacts are bridged by Zn ²⁺ ions linking His 520 of
137	one molecule (chains A, B, E and F) and the same residue in a second molecule of

PTB34 either inside or outside the asymmetric unit. In this case, the two additional ligands for Zn²⁺ are presumed to be water molecules though the electron density was too weak to incorporate them in the refined model. These zinc-mediated interactions explain why the cation is required to obtain crystals (see Materials and Methods) but, since only two of the four ligands are provided by amino acids from nPTB34, they are not considered to be physiologically significant.

NMR structure of nPTB34

The solution NMR structure of nPTB34 was obtained from a construct containing residues 325-531 and is very similar to the one used for crystallography (see Materials and Methods). Using a total of 3622 nOe derived distance restraints and 55 hydrogen bond restraints identified from slow exchanging amides we derived a fairly good ensemble of nPTB34 conformations in solution with a heavy atom RMSD of 0.71 Å of the structured region (Fig. 2a). None of the restraints were violated by more than 0.3 Å and 67% of backbone torsions of the structured residues lay in the most favored region defined by the Ramachandran plot. Due to signal overlaps and broad linewidths the loops (β 2- β 3-loops, β 4- β 5 loop RRM3) and part of the second beta strand in RRM3 could not be completely assigned. Missing assignments in β 2 of RRM3 appear to be the reason for the slightly different packing of the first alpha helix (α 1) in RRM3 against the β -sheet compared to the crystal structure. Since α 1 is part of the domain interface this different packing results also in a slight difference in the domain interface compared to the nPTB34 crystal structure and RNA bound and free PTB34 solution structures.

Comparison of Crystal and NMR structures of nPTB34

Overall there is very good correspondence between the structures of nPTB34 determined crystallographically and by NMR. Superposition of the two models using just C_a atoms gives an RMSD of 3.0 Å, and RMSDs of 1.8 and 2.6 Å for RRMs 3 and 4 respectively (Fig. 2b). These values are slightly higher than for the superposition of the crystal structure of nPTB34 onto the solution structures of PTB34 in the absence or presence of RNA, which both give overall RMSDs of 1.3 Å (Fig. 2c). This largely

169	reflects the fact that the solution structure of nPTB34 (unlike PTB34 (Vitali et al.,
170	2006)) was determined without the aid of segmental labeling and thus chemical shift
171	completeness for protons of only 77% could be achieved. The relative orientation of
172	RRMs 3 and 4 differs slightly between the crystal and solution structures of nPTB34
173	but this is unlikely to be significant since there is no significant difference in the
174	domain orientations between the crystal structure of nPTB34 and the solution
175	structure of PTB34 (see below); moreover superposition of the crystal structures of
176	the PTB34 fragments from nPTB and hnRNP-L (Zhang et al., 2013) (RMSD = 1.3 Å)
177	shows that the relative disposition of RRM3 and RRM4 is highly conserved between
178	these two proteins (Fig. 2d).
179	Within each RRM of nPTB34 there is good correspondence of secondary structure
180	features between the crystal and solution structures. Those loops in the crystal
181	structure with the highest temperature factors (RRM3 - β 2- β 3 and the C-terminal end
182	of $\beta4$ - $\beta5$; RRM4 - $\beta1$ - $\alpha2$, $\beta2$ - $\beta3$, $\alpha2$ - $\beta4$; and the inter-domain linker) are those
183	exhibiting greatest mobility in the solution structure (Fig. 2a, b). Notably, the $\beta 4\text{-}\beta 5$
184	loop is not disordered in the crystal structure of RRM2 but this may simply be
185	because it is involved in more crystal contacts (Joshi et al., 2011).
186	Within the inter-domain linker (residues 433-453), the central portion (residues 439-
187	448) exhibits considerable conformational variation in the solution structure of
188	nPTB34 (Fig. 2a). A similar but slightly smaller region (residues 443-449), which
189	protrudes away from the body of the domain, is variable between the eight chains
190	present in the asymmetric unit of the nPTB34 crystals (Fig. 1d). Again, this likely
191	reflects packing variations since there are effectively only two distinct conformers
192	evident for residues 443-449, which partition into the two distinct packing
193	environments of the pseudo P2 ₁ 2 ₁ 2 ₁ space group (see above). The N- and C-terminal
194	portions of the linker are involved in a number of specific polar and nonpolar
195	interactions that help to stabilize the packing of RRM3 and RRM4 and are described
196	in more detail below.
197	
198	Comparison of nPTB34 with PTB34

199 PTB and nPTB have 75% sequence identity overall but this is focused in the RRMs

where the sequence identity between equivalent domains ranges from 80% (RRMs 3

Structure of nPTB34 Page 8/25 Joshi et al.

201	and 4) to 88% (RRM2) (Fig. 1a). As expected, the three-dimensional structures of
202	nPTB34 and PTB34 are very similar; differences are largely confined to the local
203	effects of amino acid substitutions.
204	The crystal structure of nPTB34 reveals that the interaction between RRM3 and
205	RRM4 is stabilized by the exclusion of water molecules, which allows direct contact
206	between a conserved set of hydrophobic residues — Ile 505, Leu 508, Ile 509 and Phe
207	526 from RRM4 and the apolar portions of Ser 354, Thr 357, Leu 358, Val 361 and
208	Met 400 from RRM3 (Fig. 3a). Ringing this hydrophobic core are direct and water-
209	mediated hydrogen bonds between the RRMs and from the RRMs to the linker
210	polypeptide. Within the RRM3-RRM4 interface there are only five amino acids
211	changes between PTB34 and nPTB34 and these are generally of a conservative
212	character; the apolar residues Ile 356, Met 400 and Val 505 in PTB34 are replaced by
213	Thr 357, Leu 399 and Ile 505 respectively in nPTB34, while His 397 and His 400 in
214	PTB34 are altered to Gln 398 and Tyr 401 (Table 3). The water-mediated hydrogen
215	bond interaction from Tyr 401 of RRM3 to the side chain of Asp 501 in RRM4 of
216	nPTB34 is therefore lost in PTB34 but neither this nor the other amino acid changes
217	appear sufficient to significantly alter the interaction between the two domains. A
218	similar degree of conservation of the apolar residues at the hydrophobic interface
219	between RRM3 and RRM4 is also seen in hnRNP-L (Zhang et al., 2013) (Table 3).
220	The relative orientation of these domains is therefore a conserved feature of PTB,
221	nPTB and hnRNP-L. The incorporation of a pair of His residues within the inter-
222	domain interface of PTB34 (H397, H400) may affect the stability of the module at
223	low pH (Nordlund et al., 2003), but we are not aware of any circumstances where pH
224	regulation of the conformation would be applied.
225	Although the interaction of RRM4 with the helical face of RRM3 within PTB34 and
226	nPTB34 is much more extensive than the interaction of PTB-binding peptides in
227	Raver1 with the equivalent face of RRM2 (Joshi et al., 2011), there is one interesting
228	parallel. Superposition of the RRM2-raver1 co-crystal structure onto RRM3 of
229	nPTB34 reveals that the Raver1 peptide occupies essentially the same position as
230	helix α2 of RRM4 (Fig. 3b,c). Although the Raver1 peptide is non-helical — in fact it
231	has a pinched but largely extended conformation — it inserts a pair of Leu residues
232	(Leu 500 and Leu 501 in PDB entry 3zzy) into a hydrophobic pocket formed between

233	the helices $\alpha 1$ and $\alpha 2$ of RRM2 that effectively mimics the positioning of Ile 505 and
234	Ile 509 from RRM4 into the equivalent pocket on RRM3 within nPTB34.
235	Although the RRMs are the most highly conserved features between PTB and nPTB,
236	there are some notable differences on their RNA binding surfaces. These differences
237	appear to be more concentrated on RRM3. While there are a total of five amino acid
238	substitutions in nPTB RRM3 of residues identified to contact RNA in the solution
239	structure of the complex of PTB34 with a CUCUCU oligonucleotide (Oberstrass et
240	al., 2005), there are only two such amino acid changes in RRM4 (Fig. 4).
241	The replacement of Phe 371 in the β 2- β 3 loop of RRM3 in PTB34 by Tyr 372 in
242	nPTB34 is conservative and likely to preserve the stacking interaction with the
243	cytosine base at position 5 in CUCUCU RNA oligomer. However, the substitution of
244	As 376 (to Ser 377) at the start of the $\beta3$ strand and a triplet of replacements in the
245	$\beta 4\text{-}\beta 5$ loop (Asn 413, Gln 421 and Glu 422 in PTB34 to Thr 414, Leu 422 and
246	Asp 423 respectively in nPTB34) may modulate RNA binding (Fig. 4a). Likewise the
247	$\beta 2\text{-}\beta 3$ loop of RRM4 in PTB34 is altered in nPTB34 by deletion of Lys 489 and
248	replacement of Arg 491 by His, a pair of changes that may also alter RNA interactions
249	(Fig. 4b). The idea that these structural changes affect RNA affinity is supported by
250	mutagenesis experiments which showed that residues in the β 2- β 3 loops of RRMs 3
251	and 4 and in the β 4- β 5 loop of RRMs are important for RNA binding (Conte et al.,
252	2000; Yuan et al., 2002). The observed amino acid changes are likely to contribute to
253	the differences observed in the interactions of PTB and nPTB with larger RNA targets
254	(Pilipenko et al., 2001). However, it should not be forgotten that sequence differences
255	between PTB and nPTB are focused in regions outside the RRM domains and these
256	may well also be important for differences in splicing activity (Markovtsov et al.,
257	2000; Robinson & Smith, 2005), perhaps by recruiting different protein cofactors.
258	
259	Materials and Methods
260	Plasmid construction and protein expression and purification of nPTB34 for
261	crystal structure determination
262	The cDNA coding for residues 336-531 of nPTB were amplified by PCR and ligated
263	into the E. coli expression vector pETM-11 (Zou et al., 2003), which adds an N-

Structure of nPTB34 Page 10/25 Joshi et al.

264	terminal hexahistidine tag that could be removed using the Tobacco Etch Virus N1a
265	protease. The fragment was cloned to position the first residue (G336) as the Gly in
266	the TEV protease recognition site (ENLYFQ/G); protease processing therefore
267	removed all vector-derived amino acids.
268	Expression of nPTB34 was induced in E. coli BL21 (DE3) cells at 37°C for four
269	hours by addition of 1 mM isopropyl $\beta\text{-D-1-thiogalactopyranoside}$ (IPTG). Cells were
270	re-suspended in 0.1 M NaCl, 25 mM Tris HCl pH7.5, 0.1% Triton X-100, 0.5 mM
271	phenylmethylsulfonyl fluoride (PMSF) and 1 mg/mL lysozyme and lysed by
272	sonication. Cell debris and nucleic acid were removed by centrifugation at 25,000g
273	for 40 minutes at 4°C in the presence of 1mg/mL protamine sulfate. nPTB34 was
274	purified from the supernatant by gravity flow through TALON Metal Affinity Resin
275	(Clontech) with stepped elution. The hexahistadine tag was cleaved by addition of
276	1mg Tobacco Etch Virus N1a protease for 20 mg of nPTB34 and dialysed overnight
277	into 50 mM Tris pH7.8, containing 0.1 M NaCl, 10% glycerol, 3mM
278	β -mercaptoethanol and 0.5 μ M Ethylenediamine tetraacetic acid (EDTA). Cleaved
279	nPTB34 was purified away from the tag, uncleaved nPTB34 and N1a protease by a
280	second application to TALON resin. Proteins were further purified by size exclusion
281	chromatography on a Superdex 75 (GE Healthcare) using an ÄKTA FPLC system in
282	25 mM Tris pH 7.8, 0.1 M NaCl and 0.5 mM DTT. Peak fractions were concentrated
283	and stored at -80°C. Expression of Se-Methionine (Se-Met) labeled nPTB34 was
284	performed as above with the following differences: proteins were expressed in $E.\ coli$
285	B834 (DE3) cells in minimal media supplemented with Se-Met (Molecular
286	Dimensions). Purification proceeded as for unlabeled protein with the addition of
287	5 mM $\beta\text{-mercaptoethanol}$ to all buffers. Incorporation of Se-Met was determined to be
288	100% by MALDI-TOF mass spectrometry (data not shown).
289	
290	Crystal structure determination of nPTB34
291	Purified recombinant nPTB34 was concentrated to ≈5 mg/mL in 100 mM NaCl,
292	20 mM Tris (pH 7.8) and 0.5 mM DTT. nPTB34 was crystallised by sitting drop
293	vapor diffusion with a reservoir solution containing 0.1 M Tris (pH 8.0), 2 mM ZnCl ₂
294	and 20% polyethylene glycol (PEG) 6000. Crystals appeared at first as stacked plates,
295	but single crystals were obtained after micro-seeding into equilibrated drops of

Structure of nPTB34 Page 11/25 Joshi et al.

296	nP1B34 in 0.1 M 1ris (pH 8.0), 0.2 mW 2 nCl ₂ and 12% PEG 6000. No crystals were
297	obtained in the absence of $ZnCl_2$ — the structure revealed that this is because two
298	crystal-packing interactions are mediated by zinc ions (see results). Crystals were
299	harvested and briefly incubated in mother liquor supplemented with 20% glycerol
300	before flash cooling in liquid N_2 .
301	X-ray diffraction data were collected from a single crystal (60 μ m × 40 μ m × 20 μ m)
302	at beamline I02 at the Diamond Light Source (Didcot, UK). Diffraction data were
303	initially indexed in iMosflm and scaled in space group P2 ₁ 2 ₁ 2 using SCALA
304	(Collaborative Computer Project No. 4, 1994). Closer inspection of the data in
305	POINTLESS suggested the space group was more likely to be P2 ₁ . At this stage
306	molecular replacement was attempted in PHASER (McCoy et al., 2007) using the
307	solution structure of nPTB34 as a search model to locate the four molecules in the
308	asymmetric unit expected from the Matthews co-efficient of 2.08 Da Å ⁻³ but failed to
309	find any acceptable solutions.
310	We therefore switched to phasing by multi-wavelength anomalous dispersion (MAD)
311	using isomorphous crystals grown from Se-Met labeled nPTB34 (see above).
312	Diffraction data were collected at three wavelengths at beamline I03 at the Diamond
313	Light Source and processed in space-group P2 ₁ . Heavy atom site were identified using
314	SHELXD within autoSHARP (Bricogne et al., 2003; Vonrhein et al., 2007; Sheldrick,
315	2008) and following density modification the figure of merit was 0.802. Initial model
316	building was performed automatically in BUCCANEER (Cowtan, 2006) where two
317	nPTB34 molecules were built in the asymmetric unit. We used this initial model in
318	Phaser 2.1 to find the remaining pair of molecules in the asymmetric unit. However,
319	maps calculated using the 'completed' model remained noisy in the region
320	corresponding to this second pair of polypeptide chains and refinement stalled at an
321	R_{free} value of over 37%. At this stage the data were re-indexed in P1 and a molecular
322	replacement search performed using the tetrameric arrangement of crystallographic
323	models generated as described above was used to locate all eight 8 copies of nPTB34
324	in the larger asymmetric unit. This model refined without any further difficulty.
325	Initially, strict NCS restraints were employed during refinement in CNS v1.2
326	(Brunger et al., 1998). TLS refinement and latter cycles of refinement were performed
327	in Phenix without NCS restraints (Adams et al., 2010). Model building was performed

Structure of nPTB34 Page 12/25 Joshi et al.

328 in COOT (Emsley & Cowtan, 2004). Stereochemistry and clashes were assessed 329 using MolProbity (Adams et al., 2010). 330 331 Plasmid construction, expression and purification of nPTB34 for solution 332 structure. 333 A 207-residue C-terminal fragment (residues 325-531) of human nPTB (Swissprot 334 Q9UKA9), which contain the third and fourth RRMs, was sub-cloned into a pET-335 28a(+) vector, using the restriction sites Nde I and Not I. The sequence contained an 336 N-terminal 6xHis-tag. The proteins were over-expressed in BL21(+) E.coli cultures 337 grown in M9 minimal medium containing 50 µg/mL Kanamycin. The expression was induced by IPTG at an OD of 0.4. For ¹⁵N-labelling ¹⁵N-NH₄Cl was added as the only 338 339 nitrogen source and for ¹³C-labelling normal glucose was replaced by ¹³C labeled 340 glucose. The cell pellets were harvested by centrifugation and resuspended in lysis 341 buffer containing 300 mM NaCl, 50 mM NaH₂PO₄ and 1 mM imidazole at pH8 and 342 lysed by 3 passages through a cell-cracker (EmulsiFlex-C5 High Pressure 343 Homogenizer from Avestin, Canada). The protein was purified by two successive Ni-344 NTA columns (1ml Ni-NTA resin per liter of culture). Elution occurred between 345 40 mM and 200 mM imidazole. After the second column the protein was dialyzed 346 against the NMR buffer containing 20mM NaCl and 10 mM NaH₂PO₄ at pH 5.8 and 347 concentrated by centricon ultra centrifugation to 1 to 2 mM. The purity of the protein 348 sample was tested by SDS gels. The final yield per liter of culture was estimated to be 349 around 20 mg protein. Mass spectroscopy was used to characterize the proteins. 350 351 NMR spectroscopy 352 Shigemi NMR tubes with 250 μL sample solution (10% or 100% D₂O) were used. 353 NMR spectra were acquired at 303 K on a Bruker DRX-600 and a Avance-900 354 spectrometer. NMR data were processed using Topspin 3.0 (Bruker) and analyzed 355 using Sparky (Goddard & Kneller, 2007). 356 For the sequence specific backbone assignment HNCA, HN(CO)CA, CBCA(CO)NH, HNCACB, ¹⁵N HSQC, ¹³C HSQC as well as ¹⁵N TROSY spectra were recorded. The 357 358 aliphatic side chains were assigned based on a ¹⁵N NOESY and a ¹³C NOESY with the help of a ¹⁵N TOCSY and a HCCH-TOCSY. The assignment of side chain amides 359

was achieved by analyzing the ¹⁵N NOESY and the ¹⁵N HSQC, while for the assignment of the aromatic side chains a 2D TOCSY and a 2D NOESY in D₂O were recorded. Distance restraints used in structure calculations were extracted from ¹⁵N-NOESY-HSQC and ¹³C-NOESY-HSQC in H₂O and 2D NOESY in D₂O. Hydrogen-bonded NH groups were identified by the presence of amide resonances in ¹⁵N HSQC spectra, which were recorded immediately after lyophilizing and dissolving the sample in D₂O.

NMR structure calculation

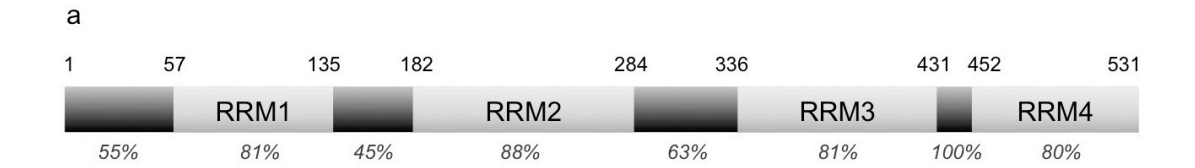
Initial peak picking and nOe assignments were performed using the ATNOSCANDID package (Herrmann, Guntert & Wuthrich, 2002b; Herrmann, Guntert & Wuthrich, 2002a). Peak lists of the final seventh cycle were used as an input for the program CYANA 3.0 (Guntert, 2004). The "noeassign" protocol of CYANA was used to reassign and calibrate the nOe signals of the given peak lists. These lists were manually reviewed and the distance restraint list were further used by CYANA to calculated 250 structures by a simulated annealing protocol (20,000 MD steps). Based on the target function the 50 best structures were selected for refinement using a simulated annealing protocol with the AMBER 9 suite (Pearlman et al., 1995) and against the ff99 force field (Lindorff-Larsen et al., 2010) using implicit water (Bashford & Case, 2000). The 20 final conformers were selected using a combined AMBER energy and violation energy as selection criteria.

Acknowledgements

We thank staff at the Diamond Light Source (Didcot, UK) for assistance with X-ray data collection. This work was supported in part by grant support from the Biotechnological and Biological Sciences Research Council (BBSRC) to SC and from SNF-NCCR Structural Biology to FHTA. AJ is grateful for the award of a BBSRC PhD studentship.

Structure of nPTB34 Page 14/25 Joshi et al.

390 Figures



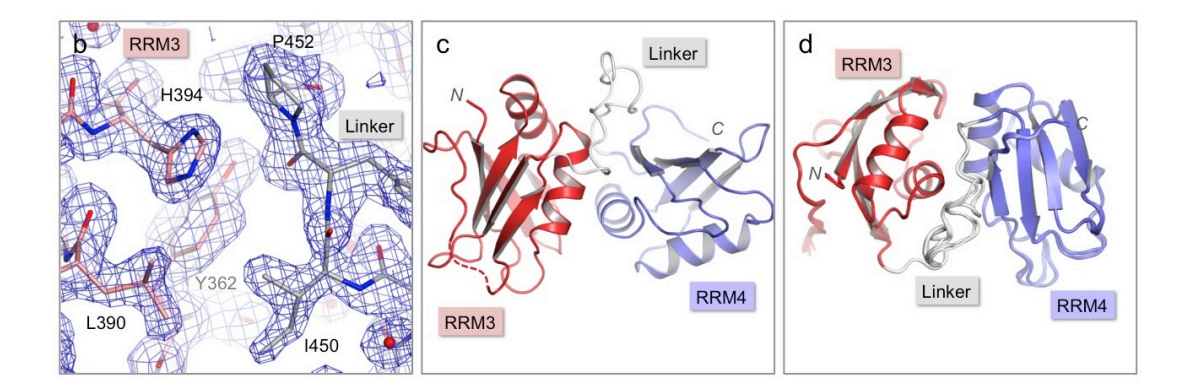


Figure 1: Crystal structure of nPTB34. (a) Domain structure of nPTB. Residue numbers for domain boundaries are given along the top; percentages below indicate the sequence identity with PTB within each defined domain or linker region. (b) 3F_o-2F_c electron density map contoured at 1σ for the refined crystal structure of nPTB34 (shown in stick representation). Carbon atoms in RRM3, RRM4 and the inter-domain linker are coloured pink, light-blue and grey respectively, a colour-scheme that is maintained throughout for nPTB34; nitrogen and oxygen atoms are coloured blue and red respectively. (c) The overall fold of the crystal structure of nPTB34 showing secondary structure features. (d) Alignment of all eight chains within the crystal asymmetric unit. View rotated with respect to panel c showing good overall alignment of secondary structure elements but differences in the linker.

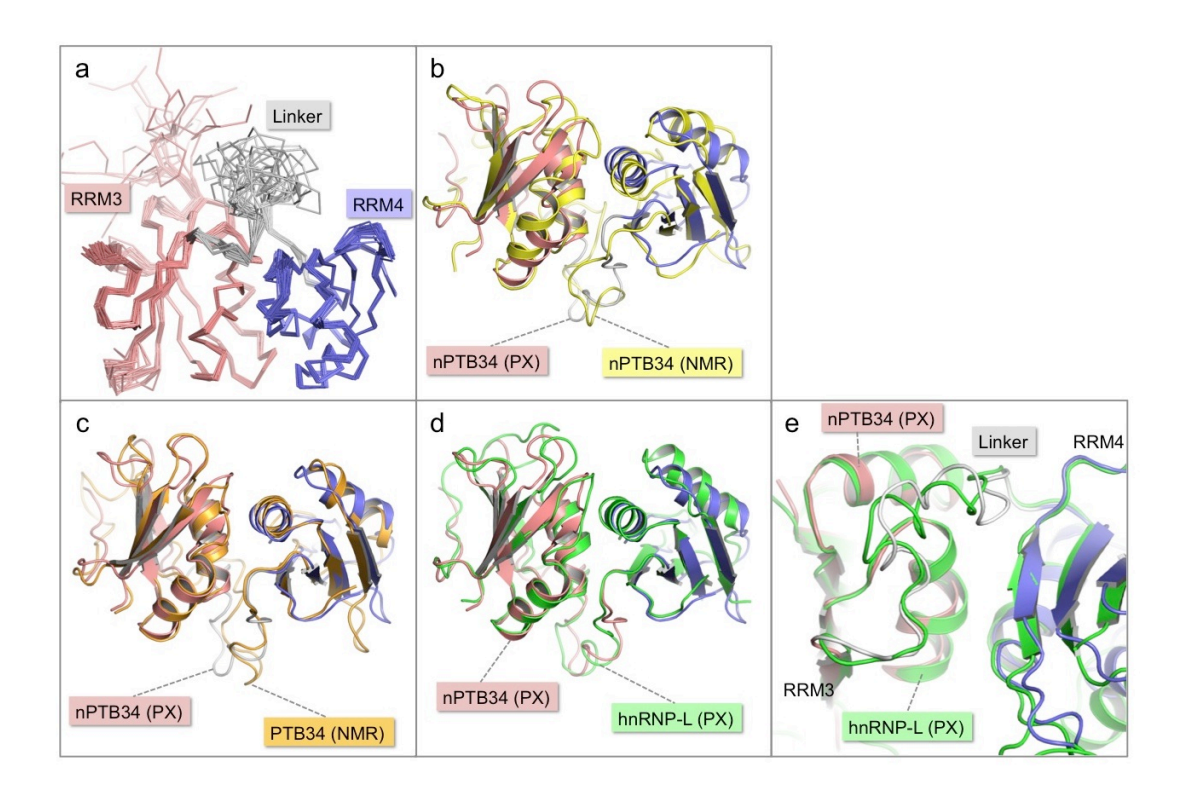


Figure 2: Solution structure of nPTB34 and comparison with related structures.

(a) Ensemble of the 20 lowest energy solution structures of nPTB34 shown as C_{α} traces coloured by domain. (b) Ribbon representation of the superposition of the crystal structure of nPTB34 (coloured by domain) on the nPTB34 solution structure (yellow). (c) Superposition of the crystal structure of nPTB34 (coloured by domain) on the solution structure of PTB34 (PDB ID 2evz; orange) (Vitali et al., 2006). (d) Superposition of the crystal structure of nPTB34 (coloured by domain) on the crystal structure of the equivalent domain from hnRNP-L (PDB ID 3to8; green) (Zhang et al., 2013). (e) Close up of the superposition shown in panel d to illustrate the similarities and differences in the linker regions between RRMs 3 and 4 in nPTB34 and hnRNP-L.

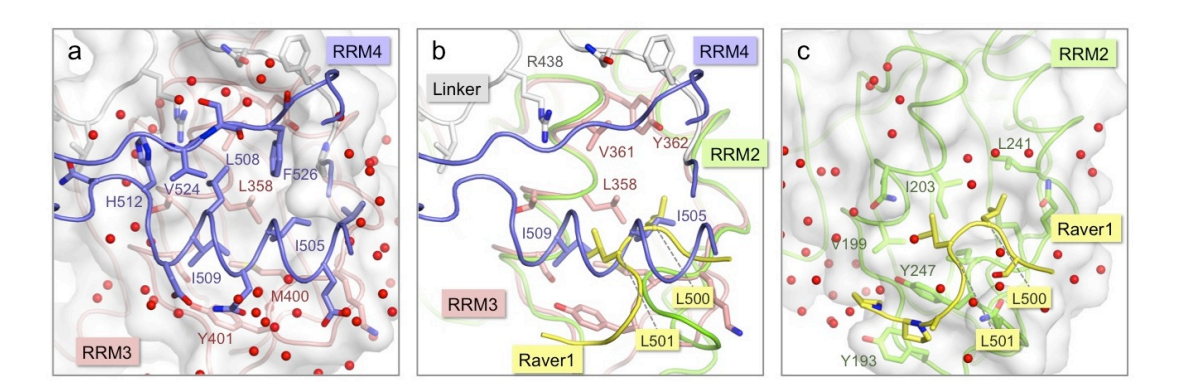
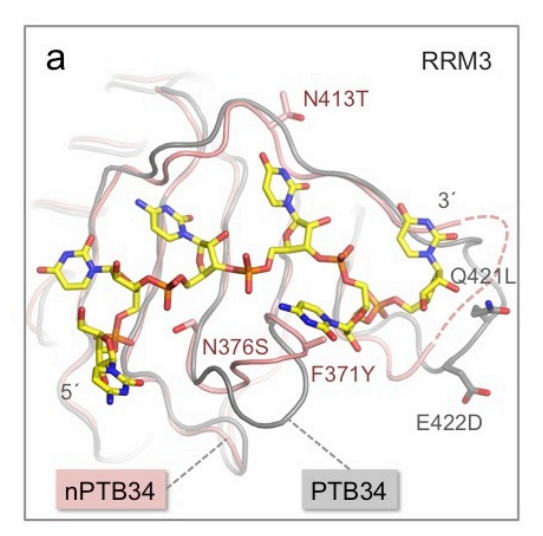
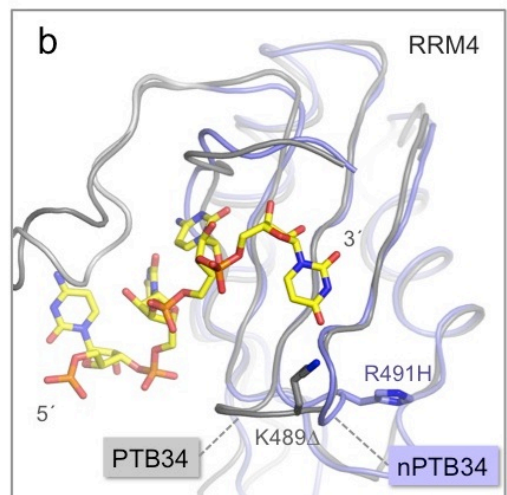


Figure 3: Comparison of the inter-domain interface within nPTB34 with the PTB RRM2-Raver1 interaction. (a) The inter-domain interface in the crystal structure of nPTB34. RRM3 is shown with pink backbone and side-chain carbon atoms along with a semi-transparent rendering of its molecular surface (light-grey). The portion of RRM4 that contacts RRM3 within nPTB34 is show without its molecular surface. The oxygen atoms of bound water molecules located in the crystal structure are indicated by red spheres. (b) Superposition of the nPTB34 crystal structure (coloured as in panel a) with the structure of the PTB RRM2-Raver1 complex (PDB ID 3zzy; RRM2 – green; Raver1 – yellow) (Joshi et al., 2011). Selected side chains are indicated. (c) The interaction between PTB RRM2 (green) and Raver1 (yellow). As for RRM3 in panel a, the molecular surface of RRM2 is indicated by a semi-transparent rendering.





436 437

438

439

440

441

442

443

444

445

446

447

448

449

450

451

452

Figure 4: Location of amino acid differences on the RNA binding surfaces of PTB34 and nPTB34. (a) Superposition of the solution structure of RRM3 from PTB34 in complex with a hexameric CUCUCU RNA oligomer (PDB ID 2adc; grey) (Oberstrass et al., 2005) onto RRM3 from the crystal structure of nPTB34 (this work; pink). The disordered portion of the β4-β5 loop in RRM3 of nPTB34 is indicated by a dashed line. The side chains of amino acids that differ between the two structures (discussed in the text) are labeled to indicate the change from PTB34 to nPTB34 and shown, where possible, for nPTB34 (note that the Tyr side chain of the F317Y substitution is disordered in the crystal structure); the two amino acid differences that occur in a disordered loop of nPTB34 RRM3 are indicated by showing their positions and conformations of their side chains in PTB34 RRM3 (Q421, E422). (b) Superposition of the solution structure of RRM4 with the hexameric CUCUCU RNA oligomer from (PDB ID 2adc; grey) with RRM4 from the nPTB34 crystal structure (this work; light-blue). To avoid cluttering the figure only the four RNA nucleotides that make contact with RRM4 are shown. The side chains of amino acids that differ between the two structures are shown for the substitution R491H and the deletion of Lys 489 (PTB34) in nPTB34, which is labeled K491Δ.

453 454

456 **References**

- 457 Adams PD, Afonine PV, Bunkoczi G, Chen VB, Davis IW, Echols N, Headd JJ,
- Hung LW, Kapral GJ, Grosse-Kunstleve RW et al. . 2010. PHENIX: a
- comprehensive Python-based system for macromolecular structure solution. *Acta*
- 460 *Cryst D* 66:213-221.
- 461 Bashford D, and Case DA. 2000. Generalized born models of macromolecular
- solvation effects. *Annual review of physical chemistry* 51:129-152.
- Boutz PL, Stoilov P, Li Q, Lin C-H, Chawla G, Ostrow K, Shiue L, Ares M, and
- Black DL. 2007. A post-transcriptional regulatory switch in polypyrimidine tract-
- binding proteins reprograms alternative splicing in developing neurons. Genes
- 466 Dev 21:1636-1652.
- Bricogne G, Vonrhein C, Flensburg C, Schiltz M, and Paciorek W. 2003. Generation,
- representation and flow of phase information in structure determination: recent
- developments in and around SHARP 2.0. Acta Cryst D 59:2023-2030.
- 470 Brunger AT, Adams PD, Clore GM, DeLano WL, Gros P, Grosse-Kunstleve RW,
- Jiang JS, Kuszewski J, Nilges M, Pannu NS et al. . 1998. Crystallography & NMR
- system: A new software suite for macromolecular structure determination. Acta
- 473 *Cryst D* 54:905-921.
- 474 Clerte C, and Hall KB. 2006. Characterization of multimeric complexes formed by
- the human PTB1 protein on RNA. RNA (New York, NY) 12:457-475.
- 476 Collaborative Computer Project No. 4. 1994. The CCP4 suite: programs for protein
- 477 crystallography. *Acta Cryst D* 50:760-763.
- 478 Conte MR, Grüne T, Ghuman J, Kelly G, Ladas A, Matthews S, and Curry S. 2000.
- Structure of tandem RNA recognition motifs from polypyrimidine tract binding
- protein reveals novel features of the RRM fold. *EMBO J* 19:3132-3141.
- Cowtan K. 2006. The Buccaneer software for automated model building. 1. Tracing
- 482 protein chains. *Acta Cryst D* 62:1002-1011.
- Emsley P, and Cowtan K. 2004. Coot: model-building tools for molecular graphics.
- 484 *Acta Cryst D* 60:2126-2132.
- García-Blanco MA, Jamison SF, and Sharp PA. 1989. Identification and purification
- of a 62,000-dalton protein that binds specifically to the polypyrimidine tract of
- 487 introns. Genes Dev 3:1874-1886.

- 488 Gil A, Sharp PA, Jamison SF, and Garcia-Blanco MA. 1991. Characterization of
- cDNAs encoding the polypyrimidine tract-binding protein. Genes Dev 5:1224-
- 490 1236.
- 491 Goddard TD, and Kneller DG. 2007. SPARKY 3.114. San Francisco: University of
- 492 California.
- 493 Gooding C, Kemp P, and Smith CWJ. 2003. A novel polypyrimidine tract-binding
- protein paralog expressed in smooth muscle cells. *J Biol Chem* 278:15201-15207.
- 495 Guntert P. 2004. Automated NMR structure calculation with CYANA. Methods in
- 496 *molecular biology* 278:353-378.
- 497 Herrmann T, Guntert P, and Wuthrich K. 2002a. Protein NMR structure
- determination with automated NOE assignment using the new software CANDID
- and the torsion angle dynamics algorithm DYANA. Journal of molecular biology
- 500 319:209-227.
- 501 Herrmann T, Guntert P, and Wuthrich K. 2002b. Protein NMR structure
- determination with automated NOE-identification in the NOESY spectra using the
- new software ATNOS. *Journal of biomolecular NMR* 24:171-189.
- Joshi A, Coelho MB, Kotik-Kogan O, Simpson PJ, Matthews SJ, Smith CW, and
- Curry S. 2011. Crystallographic analysis of polypyrimidine tract-binding protein-
- raver1 interactions involved in regulation of alternative splicing. Structure
- 507 19:1816-1825.
- Lamichhane R, Daubner GM, Thomas-Crusells J, Auweter SD, Manatschal C, Austin
- KS, Valniuk O, Allain FH-T, and Rueda D. 2010. RNA looping by PTB:
- Evidence using FRET and NMR spectroscopy for a role in splicing repression.
- Proceedings of the National Academy of Sciences of the United States of America
- 512 107:4105-4110.
- Laskowski RA, Rullmannn JA, MacArthur MW, Kaptein R, and Thornton JM. 1996.
- AQUA and PROCHECK-NMR: programs for checking the quality of protein
- structures solved by NMR. *Journal of biomolecular NMR* 8:477-486.
- Lindorff-Larsen K, Piana S, Palmo K, Maragakis P, Klepeis JL, Dror RO, and Shaw
- DE. 2010. Improved side-chain torsion potentials for the Amber ff99SB protein
- force field. *Proteins* 78:1950-1958.
- Llorian M, Schwartz S, Clark TA, Hollander D, Tan L-Y, Spellman R, Gordon A,
- Schweitzer AC, De La Grange P, Ast G et al. . 2010. Position-dependent

PeerJ PrePrints

- alternative splicing activity revealed by global profiling of alternative splicing
- events regulated by PTB. Nat Struct Mol Biol.
- Markovtsov V, Nikolic JM, Goldman JA, Turck CW, Chou MY, and Black DL. 2000.
- Cooperative assembly of an hnRNP complex induced by a tissue-specific
- homolog of polypyrimidine tract binding protein. *Mol Cell Biol* 20:7463-7479.
- Maynard CM, and Hall KB. 2010. Interactions between PTB RRMs induce slow
- 527 motions and increase RNA binding affinity. Journal of molecular biology
- 528 397:260-277.
- McCoy AJ, Grosse-Kunstleve RW, Adams PD, Winn MD, Storoni LC, and Read RJ.
- 530 2007. Phaser crystallographic software. *J App Crystallogr* 40:658-674.
- Nilsen TW, and Graveley BR. 2010. Expansion of the eukaryotic proteome by
- alternative splicing. *Nature* 463:457-463.
- Nordlund HR, Hytönen VP, Laitinen OH, Uotila STH, Niskanen EA, Savolainen J,
- Porkka E, and Kulomaa MS. 2003. Introduction of histidine residues into avidin
- subunit interfaces allows pH-dependent regulation of quaternary structure and
- biotin binding. *FEBS letters* 555:449-454.
- Oberstrass FC, Auweter SD, Erat M, Hargous Y, Henning A, Wenter P, Reymond L,
- Amir-Ahmady B, Pitsch S, Black DL et al. . 2005. Structure of PTB bound to
- RNA: specific binding and implications for splicing regulation. *Science* 309:2054-
- 540 2057.
- Pearlman DA, Case DA, Caldwell JW, Ross WS, Cheatham III TE, DeBolt S,
- Ferguson D, Seibel G, and Kollman P. 1995. AMBER, a package of computer
- programs for applying molecular mechanics, normal mode analysis, molecular
- dynamics and free energy calculations to simulate the structural and energetic
- properties of molecules. *Computer Physics Communications* 91:1-41.
- Pérez I, Lin CH, McAfee JG, and Patton JG. 1997. Mutation of PTB binding sites
- causes misregulation of alternative 3' splice site selection in vivo. RNA 3:764-778.
- Petoukhov MV, Monie TP, Allain FH, Matthews S, Curry S, and Svergun DI. 2006.
- Conformation of polypyrimidine tract binding protein in solution. Structure
- 550 14:1021-1027.
- 551 Pilipenko EV, Viktorova EG, Guest ST, Agol VI, and Roos RP. 2001. Cell-specific
- proteins regulate viral RNA translation and virus-induced disease. EMBO J
- 553 20:6899-6908.

- Polydorides AD, Okano HJ, Yang YY, Stefani G, and Darnell RB. 2000. A brain-
- enriched polypyrimidine tract-binding protein antagonizes the ability of Nova to
- regulate neuron-specific alternative splicing. Proc Natl Acad Sci USA 97:6350-
- 557 6355.
- Rideau AP, Gooding C, Simpson PJ, Monie TP, Lorenz M, Hüttelmaier S, Singer RH,
- Matthews S, Curry S, and Smith CWJ. 2006. A peptide motif in Raver1 mediates
- splicing repression by interaction with the PTB RRM2 domain. *Nature structural*
- *& amp; molecular biology* 13:839-848.
- Robinson F, and Smith CW. 2005. A splicing repressor domain in polypyrimidine
- tract binding protein. *J Biol Chem*.
- Sawicka K, Bushell M, Spriggs KA, and Willis AE. 2008. Polypyrimidine-tract-
- binding protein: a multifunctional RNA-binding protein. Biochem Soc Trans
- 566 36:641-647.
- 567 Sharma S, Falick AM, and Black DL. 2005. Polypyrimidine tract binding protein
- blocks the 5' splice site-dependent assembly of U2AF and the prespliceosomal E
- 569 complex. *Mol Cell* 19:485-496.
- 570 Sheldrick GM. 2008. A short history of SHELX. *Acta Cryst A* 64:112-122.
- 571 Simpson PJ, Monie TP, Szendröi A, Davydova N, Tyzack JK, Conte MR, Read CM,
- Cary PD, Svergun DI, Konarev PV et al. . 2004. Structure and RNA interactions
- of the N-terminal RRM domains of PTB. Structure 12:1631-1643.
- 574 Singh R, Valcárcel J, and Green MR. 1995. Distinct binding specificities and
- functions of higher eukaryotic polypyrimidine tract-binding proteins. Science
- 576 268:1173-1176.
- 577 Spellman R, Llorian M, and Smith CWJ. 2007. Crossregulation and functional
- redundancy between the splicing regulator PTB and its paralogs nPTB and ROD1.
- 579 *Mol Cell* 27:420-434.
- Vitali F, Henning A, Oberstrass FC, Hargous Y, Auweter SD, Erat M, and Allain FH-
- T. 2006. Structure of the two most C-terminal RNA recognition motifs of PTB
- using segmental isotope labeling. *EMBO J* 25:150-162.
- Vonrhein C, Blanc E, Roversi P, and Bricogne G. 2007. Automated structure solution
- with autoSHARP. *Methods Mol Biol* 364:215-230.
- Witten JT, and Ule J. 2011. Understanding splicing regulation through RNA splicing
- 586 maps. *Trends Genet* 27:89-97.

587	Xue Y, Zhou Y, Wu T, Zhu T, Ji X, Kwon Y-S, Zhang C, Yeo G, Black DL, Sun H et
588	al 2009. Genome-wide analysis of PTB-RNA interactions reveals a strategy
589	used by the general splicing repressor to modulate exon inclusion or skipping. Mol
590	Cell 36:996-1006.
591	Yamamoto H, Tsukahara K, Kanaoka Y, Jinno S, and Okayama H. 1999. Isolation of
592	a mammalian homologue of a fission yeast differentiation regulator. Mol Cell Biol
593	19:3829-3841.
594	Yuan X, Davydova N, Conte MR, Curry S, and Matthews S. 2002. Chemical shift
595	mapping of RNA interactions with the polypyrimidine tract binding protein.
596	Nucleic Acids Res 30:456-462.
597	Zhang W, Zeng F, Liu Y, Zhao Y, Lv H, Niu L, Teng M, and Li X. 2013. Crystal
598	structures and RNA-binding properties of the RNA recognition motifs of
599	heterogeneous nuclear ribonucleoprotein L: insights into its roles in alternative
600	splicing regulation. Journal of Biological Chemistry 288:22636-22649.
601	Zou P, Gautel M, Geerlof A, Wilmanns M, Koch MHJ, and Svergun DI. 2003.
602	Solution scattering suggests cross-linking function of telethonin in the complex
603	with titin. J Biol Chem 278:2636-2644.

Table 1: Crystal structure — data collection and refinement statistics

DATA COLLECTION	Native nPTB34	Se-Met labeled nPTB34		
Space-group	P1	P2 ₁		
a, b, c (Å)	60.98, 65.81, 99.55	65.81, 60.95, 99.55		
α, β, γ (°)	89.99, 90.00, 90.00	90.00, 90.01, 90.00		
		Peak	Inflection	Remote
Wavelength (Å)	0.9795	0.9808	0.9813	0.9790
Resolution range (Å)	44.83-1.69	55.10-2.30	55.14-2.30	55.27-2.50
Resolution range (A)	(1.78-1.69)	(2.42-2.30)	(2.42-2.30)	(2.64-2.50)
No. of independent reflections	150219 (20577)	-	-	-
Multiplicity ¹	1.9 (1.9)	1.7 (1.6)	1.7 (1.7)	1.7 (1.7)
Completeness (%)	86.4 (81.0)	89.9 (84.8)	95.9 (96.1)	95.7 (93.5)
I/σ_I	4.2 (1.5)	10.0 (4.3)	8.7 (3.0)	8.1 (2.4)
$R_{\text{merge}} (\%)^2$	8.8 (54.4)	6.7 (21.2)	8.6 (37.9)	9.4 (47.8)
MODEL REFINEMENT				
No. of Non-hydrogen atoms/waters	12571			
$\mathbf{R}_{\mathrm{model}}\left(\%\right)^{3}$	22.8			
R _{free} (%) ⁴	27.4			
RMSD bonds (Å) ⁵	0.009			
RMSD bond angles (°)	1.296			
Ramachandran plot (% favoured/allowed)	97.4/1.9			
PDB Identifier	4cko			

606

607 Values for highest resolution shell given in parentheses

608 ${}^{2}R_{merge} = 100 \times \Sigma_{hkl} |I_{j}(hkl) - \langle I_{j}(hkl) \rangle |/ \Sigma_{hkl} \Sigma_{j} I(hkl)$, where $I_{j}(hkl)$ and $\langle I_{j}(hkl) \rangle$ are the intensity of measurement j and the mean intensity for the reflection with indices hkl,

610 respectively.

 $611 \qquad {}^{{}^{3}}\!R_{work} = 100 \times \! \Sigma_{hkl} ||F_{obs}| - |F_{calc}||/\! \Sigma_{hkl} ||F_{obs}|. \label{eq:resolvent_policy}$

 $^{4}R_{\text{free}}$ is the R_{model} calculated using a randomly selected 5% sample of reflection data

that were omitted from the refinement.

614 ⁵RMSD, root-mean-squared deviations.

Table 2: Statistics for the solution structure of nPTB34

Table 2: Statistics for the solution structure of h	
Number of Distance Restraints	3677
intraresidual	657
sequential (li-jl=1)	941
medium range (1< i-j <5)	684
long range (li-jl>=5)	134
hydrogen bonds ¹	55
nydrogen bonds	33
Energy Statistics ²	
Average distance constraint violations (Å)	
0.1-0.2 Å	52.4 +/- 4.2
0.2-0.3 Å	0.4 +/- 0.6
>0.3 A	0.0 +/- 0.0
Maximal (Å)	0.20 +/- 0.03
Mean AMBER distance violation Energy (kcal	100.9 +/-2.5
mol^{-1})	
Mean AMBER Energy (kcal mol ⁻¹)	-6170.0 +/- 15.5
Mean Deviation from ideal covalent geometry	
Bond Length (A)	0.0042 +/-
	0.0000
Bond Angle (degrees)	1.796 +/- 0.007
Ramachandran plot Statistics ^{2,3,4}	
Most favoured regions (%)	67.1 +/- 2.0
Additionally allowed regions (%)	29.2 +/- 1.9 3.5 +/- 0.8
Generously allowed regions (%)	0.1 +/- 0.2
Disallowed regions (%)	0.1 +/- 0.2
RMS Deviations from mean structure	
Statistics ^{2,3}	
Backbone atoms (Å)	0.37 +/- 0.05
Heavy atoms (Å)	0.71 +/- 0.05
, weens (12)	3.71 17 0.05
PDB identifier	To be deposited

617

618 ¹Hydrogen bond constraints were identified from slow exchanging amide

619 protons in D_2O .

²Statistics computed for the deposited bundle of 20 violation energy best

structures selected out of 30 energy best structures refined in Amber

622 (Pearlman et al., 1995).

623 ³Based on structured residue range as defined by cyana command

624 overlay: 9-47, 52-86, 91-113, 126-163, 168-207.

⁴Ramachandran plot, as defined by the Procheck (Laskowski et al.,

626 1996).

Table 3: Conservation of amino acids within the interface between RRM3-RRM4 in

628 PTB, nPTB and hnRNP-L

629

	PTB	nPTB	hnRNP-L
RRM3			
	S353	S354	R398
	I356	T357	N401
	L357	L358	V402
	V360	V361	L405
	Y361	Y362	Y406
	Н397	Q398	N442
	L399	M400	M444
	H400	Y401	F445
RRM4			
	V501	V501	K552
	V505	1505	L556
	L508	L508	L559
	1509	1509	G560
	F526	F526	F582